Development of bead-spring polymer models using the constant extension ensemble

Patrick T. Underhill and Patrick S. Doyle[a)]

Department of Chemical Engineering, Massachusetts Institute of Technology, Cambridge, Massachusetts 02139-4307

(Received 23 November 2004; final revision received 24 June 2005)

Synopsis

We have examined a new method for generating coarse-grained models of polymers. The resulting models consist of bead-spring chains with the spring force law taken from the force-extension behavior in the constant extension ensemble. This method, called the polymer ensemble transformation method, is applied to the freely jointed chain. The resulting model illustrates why current bead-spring chain models are insufficient in describing polymer behavior at high discretization. Applying the method to the freely jointed chain with unequal rod lengths showed the effect of varying flexibility in the chain. The method was also used to generate a bead-spring model of F-actin, which shows how the method is not restricted to one molecular model and can even be applied to experimental data. The current limitations of the method are discussed, including the need for approximate bending potentials to model the worm-like chain with a bead-spring chain. We discuss practical issues such as using the bead-spring models in Brownian dynamics simulations and develop a simple spring force law that can accurately represent a freely jointed chain with only a few rods per spring. Because of the functional form of this new force law, existing computer simulations can be easily modified. © *2005 The Society of Rheology.* [DOI: 10.1122/1.2008294]

I. INTRODUCTION

Polymer kinetic theory (Bird *et al.*, 1987) has become an important tool to understand rheology of polymers as well as to understand single polymer molecule experiments [Doyle *et al.* (2000), Hur *et al.* (2000); Larson *et al.* (1997)]. The most detailed models typically used to study flow properties are the freely-jointed chain (FJC) [Flory (1989)] and Kratky-Porod [Kratky and Porod (1949)] models. These models assume that the polymer at smaller length scales remains at local equilibrium. The remaining effect of the atomistic makeup of the polymer is the determination of the Kuhn length or persistence length. Within this assumption of local equilibrium these detailed models would presumably have the desired accuracy but are computationally intractable for the long polymers and long time scales of interest. A reduction of the degrees of freedom is possible if these models are coarse-grained further to bead-spring chains.

Initially few springs were used and the polymers contained many persistence lengths so the spring force laws were obtained by examining the behavior of the detailed models for very large number of persistence lengths. This led to the derivation of the Marko and

[a)]Author to whom all correspondence should be addressed; electronic mail: pdoyle@mit.edu

Siggia interpolation formula [Marko and Siggia (1995)] and the inverse Langevin force law. Comparison with single molecule experiments have shown that the global behavior of long molecules is well approximate by these force laws in the so-called entropic region [Bustamante *et al.* (1994)]. Recently, it has become more common to use a larger number of springs. When modeling a polymer with the same contour length with a larger number of springs, a spring must represent a smaller segment of polymer. To date, these submolecules are still being modeled with the Marko and Siggia or inverse Langevin force law. However, this has been shown to be in error if each submolecule no longer contains a large enough number of Kuhn lengths or persistence lengths [Underhill and Doyle (2004)].

If each spring is chosen to model only a few Kuhn lengths of a freely jointed chain, the necessary force law can look strange compared to conventional spring force laws. This may seem confusing if the whole polymer contains many Kuhn lengths. Consider, for example, a freely jointed chain with 200 rods. If one examined the average force as a function of extension for the whole chain, it would be very close to the inverse Langevin function. However, if one models this polymer with a bead-spring chain containing 100 springs, the spring force law needed for each spring is dramatically different from the inverse Langevin function. Not only is this strange force law needed to model the behavior of the freely jointed chain on the scale of two rods, but also it is necessary in order to get the correct overall force-extension behavior and rheological behavior for the whole chain.

The increase in the number of springs is not simply motivated by increasing computation power, but may be necessary to capture essential physics of interest. Increasing the number of springs increases the number of relaxation modes of the polymer and distributes the viscous drag more evenly along the contour. In addition, recently a number of applications have surfaced with microdevices in which the behavior of the polymer at a smaller length scale is of critical importance [Doyle *et al.* (2002); Jendrejack *et al.* (2003); Han and Craighead (2000)]. Accurately modeling this behavior *requires* having a coarse-grained model that can reproduce the behavior at that length scale quantitatively yet also is computationally tractable.

Here we discuss how to systematically determine the spring force law that should be used if each spring does not represent a large number of Kuhn lengths. In this way we bridge the gap between detailed models such as the FJC and Kratky-Porod, and bead-spring chains with a large number of persistence lengths per spring. While these models will be guaranteed to reproduce some specified property of the polymer, note that if a large number of beads is used, they may still not be computationally feasible. Our approach will start from a model such as the FJC and determine the spring force law needed for a bead-spring chain model *without* assuming each spring represents a large number of Kuhn steps. We will apply this method to a number of "toy problems." Each of these examples illustrates an important point about coarse-graining into bead-spring chains.

We also discuss some practical issues of using these force laws. In some situations it may be easier to use models that are not accurate in all situations. For example, if long flexible polymers are near equilibrium, Hookean springs are sufficient to capture the response. For long DNA, freely jointed chains can capture much of general response over large length scales except gives different approaches towards full extension. Other types of approximations include things like using the FENE or Cohen force laws [Warner, (1972); Cohen (1991)] as approximations of the inverse-Langevin function or using rigid rods (constraints) instead of very stiff Fraenkel springs.

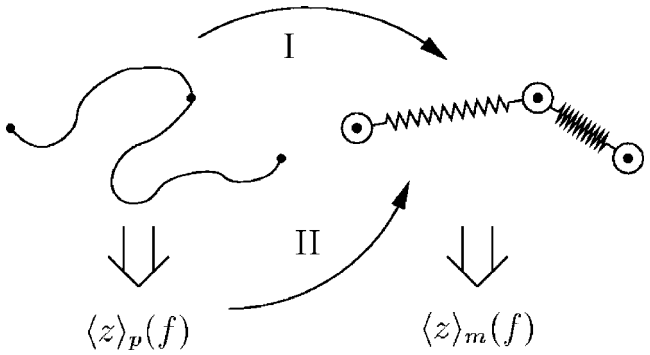

FIG. 1. There are multiple paths to build a bead-spring model. The goal of coarse-graining is to produce a model such that its behavior, $\langle z \rangle_m(f)$, matches the polymer's behavior, $\langle z \rangle_p(f)$. The paths (arrows) represent different methods of taking a property of the polymer to be the spring force law. The PET method introduced here, path I, uses the constant extension polymer behavior as the spring force law. The conventional method, path II, uses the constant force behavior as the spring force law.

II. METHOD

The general method we will be using was first introduced by Underhill and Doyle (2004). For completeness we give here a brief review of the method and its justification. An overview of the coarse-graining approach is shown in Fig. 1, comparing it with the current bead-spring chain models. We require that the model behaves identically when placed in the same external environment. The behavior we consider here is the force-extension behavior in the constant force ensemble (how much the molecule extends under application of a constant force), $\langle z \rangle(f)$. The Marko and Siggia and inverse Langevin force laws correspond to using directly the constant force behavior of the polymer. Our method instead uses the constant extension behavior of the polymer, so we call it the polymer ensemble transformation (PET) method.

While one reason the constant force ensemble was used previously to obtain a spring force law is the ability to perform analytic calculations, it may be comforting that the very behavior trying to be modeled (the constant force response) is used directly in building the bead-spring model. In fact, it may seem counterintuitive to use the constant extension ensemble to build the bead-spring chain considering both the real polymer and the beads in the model are free to move. The resolution of this paradox is illustrated pictorially in Fig. 2.

We first note that the behavior of the polymer is an average over all possible configurations. Consider performing that average by choosing a series of reference points on the polymer where the beads in the bead-spring model will be (shown by black circles in Fig. 2) and separate all the polymer configurations into categories for which each category has fixed reference points. First the average is performed within each category, for which the reference points *are* fixed, thus the constant extension ensemble is needed. In this way we replace each category (which contains many configurations) by a single configuration of the bead-spring chain.

We can show mathematically that this method works by examining the partition function of the polymer. If the bead-spring chain produced has the same partition function as the polymer being modeled, then the model will reproduce the polymer behavior. This is similar to coarse-graining from quantum chemistry calculations to repeat unit level mod-

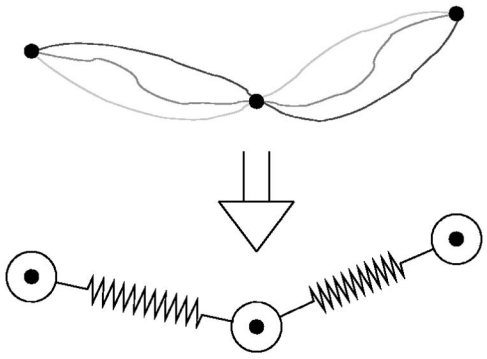

FIG. 2. The physical justification for the PET method is based on sorting all configurations of the polymer into categories. Within each category the reference points (black circles) are held fixed. The lines signify different polymer configurations within the category. When performing the average over the configurations in a category, the segment between reference points is effectively in the constant extension ensemble. This segment is replaced by a spring in the bead-spring model.

els using the distribution function of the detailed model to determine the potential energy of the coarser model [Baschnagel *et al.* (2000)]. The partition function of the polymer in the constant force ensemble is

$$\mathcal{Z}(\mathbf{f}) = \int \exp\left[\frac{-U + \mathbf{f}\cdot\mathbf{R}_{\text{tot}}}{k_B T}\right] d\mathbb{V}, \tag{1}$$

where U is the total internal energy, $\mathbf{f}$ is the constant external force applied to the end of the polymer, $\mathbf{R}_{\text{tot}}$ is the total end-to-end vector of the polymer, k_B is the Boltzmann's constant, T is the absolute temperature, and the integral is taken over all configuration space of the polymer.

For simplicity, let us first examine the development of a single spring (dumbbell) model. By using a Dirac delta function we can introduce the new variable $\mathbf{r}$ and can rewrite the partition function as

$$\mathcal{Z}(\mathbf{f}) = \int \Omega(\mathbf{r}) \exp\left[\frac{\mathbf{f}\cdot\mathbf{r}}{k_B T}\right] d\mathbf{r}, \tag{2}$$

where

$$\Omega(\mathbf{r}) = \int \exp\left[\frac{-U}{k_B T}\right] \delta(\mathbf{r} - \mathbf{R}_{\text{tot}}) d\mathbb{V} \tag{3}$$

is the constant extension ensemble partition function for which the end-to-end vector is held constant at $\mathbf{r}$. One can verify this equivalence by inserting Eq. (3) into Eq. (2) and doing the $\mathbf{r}$ integral. The partition function in Eq. (2) is of the same form as the partition function for a single dumbbell, which is given by

$$\mathcal{Z}(\mathbf{f}) = \int \exp\left[\frac{-U_s(\mathbf{r})}{k_B T}\right] \exp\left[\frac{\mathbf{f}\cdot\mathbf{r}}{k_B T}\right] d\mathbf{r}. \tag{4}$$

If the spring potential energy in the dumbbell is

$$U_s(\mathbf{r}) = -k_B T \ln \Omega(\mathbf{r}), \tag{5}$$

then the model will have the same partition function (and thus equilibrium behavior) as the real polymer. This forms the basis of the PET method, in which the constant extension ensemble behavior of the polymer is used to produce the bead-spring model. While this was a derivation for a single dumbbell model, a similar procedure can be used for chains. Each of the spring coordinates can be introduced into the polymer partition function using Dirac delta functions. For example, if two springs were desired then after the appropriate transformation the partition function would be

$$\mathcal{Z}(\mathbf{f}) = \int \Omega(\mathbf{r}_1, \mathbf{r}_2) \exp\left[\frac{\mathbf{f} \cdot (\mathbf{r}_1 + \mathbf{r}_2)}{k_B T}\right] d\mathbf{r}_1 d\mathbf{r}_2, \tag{6}$$

where $\Omega(\mathbf{r}_1, \mathbf{r}_2)$ is the partition function of the true polymer given that the vector connecting the beginning to the midpoint of the contour length is held at $\mathbf{r}_1$, and the vector connecting the midpoint to the end is held at $\mathbf{r}_2$. The partition function for a two spring chain is

$$\mathcal{Z}(\mathbf{f}) = \int \exp\left[\frac{-U_s(\mathbf{r}_1, \mathbf{r}_2)}{k_B T}\right] \exp\left[\frac{\mathbf{f} \cdot (\mathbf{r}_1 + \mathbf{r}_2)}{k_B T}\right] d\mathbf{r}_1 d\mathbf{r}_2, \tag{7}$$

where $U_s(\mathbf{r}_1, \mathbf{r}_2)$ is the potential energy of having spring 1 with connector vector $\mathbf{r}_1$ and spring 2 with connector vector $\mathbf{r}_2$. Note that this energy is not necessarily decoupled into independent contributions for each spring. Again we see that if we take

$$U_s(\mathbf{r}_1, \mathbf{r}_2) = -k_B T \ln \Omega(\mathbf{r}_1, \mathbf{r}_2), \tag{8}$$

then the bead-spring chain model will have the same equilibrium behavior as the true polymer.

While we have shown that the PET method generates a bead-spring chain that has the same constant force ensemble partition function as the true polymer, it is not obvious whether models with more than a single spring will have the same behavior as the polymer in the constant extension ensemble. In fact, there *is* a one-to-one correspondence between the two partition functions that guarantees that the model will have the correct constant extension behavior. Writing the partition function for an imaginary force, we see the integral is a Fourier transform

$$\mathcal{Z}(ik_B T\mathbf{k}) = \int \Omega(\mathbf{r}) \exp\left[i\mathbf{k} \cdot \mathbf{r}\right] d\mathbf{r}. \tag{9}$$

The constant extension partition function is therefore given by the inverse Fourier transform

$$\Omega(\mathbf{r}) = \left(\frac{1}{2\pi}\right)^d \int \mathcal{Z}(ik_B T\mathbf{k}) \exp\left[-i\mathbf{k} \cdot \mathbf{r}\right] d\mathbf{k}, \tag{10}$$

where d is the dimensionality of the vectors. Thus using the general PET method summarized in Eq. (8) reproduces the polymer behavior in both constant force and constant extension ensembles.

Looking at the relation between the constant extension and constant force partition functions, we see that they are related analogously to other conjugate ensembles such as the microcanonical and canonical ensembles [Pathria (1996)]. There has been recent interest in the constant extension and force ensembles, including what constitutes a "large system" so the ensembles are equivalent and what concepts from thermodynamics do not

apply for the single molecule analysis [Keller *et al.* (2003)]. While our work here also discusses the two ensembles, it is different from previous discussions. Most previous researchers studying these ensembles are discussing them in the context of comparison with stretching experiments of single molecules. Depending on the constraints imposed in the experiment, a different ensemble can be appropriate for the analysis. We have shown that when *coarse-graining*, the spring force law should be taken from the constant extension ensemble so that the coarse-grained model has the same response as the polymer under all constraints.

III. RESULTS AND DISCUSSION

A. Freely jointed chain

The first model we discuss is the freely jointed chain in order to review the simplest application of the method. The largest difficulty in calculating the spring force needed to model a polymer is determining the partition function $\Omega(\mathbf{r}_1,\mathbf{r}_2,\ldots)$. Because there is a great simplification in this calculation for the freely jointed chain polymer, we consider it here. The result, called the random walk spring (RWS) model, is a *collection* of spring force laws in which the form of the spring force depends on the number of Kuhn lengths represented by each spring.

It is well-known that the probability distribution of a chain with infinitely stiff Fraenkel springs is the random walk distribution [Bird *et al.* (1987)]. This is the system that we call here the freely jointed chain. A system with rods as rigid constraints without a corrective metric force would have correlations between rods resulting in a distribution different from the random walk distribution. We do not consider this case here.

The calculation of the partition function, $\Omega(\mathbf{r}_1,\mathbf{r}_2,\ldots)$, for the FJC is simplified because the joints correspond to free hinges. This decoupling between the segments of the polymer causes the partition function to be separable into a product of partition functions:

$$\Omega(\mathbf{r}_1,\mathbf{r}_2,\ldots)=\Omega(\mathbf{r}_1)\Omega(\mathbf{r}_2)\cdots. \tag{11}$$

Because the spring potential is chosen from the logarithm of the partition function, the spring potential becomes a sum over each spring (with no cross terms)

$$U_s(\mathbf{r}_1,\mathbf{r}_2,\ldots)=U_s(\mathbf{r}_1)+U_s(\mathbf{r}_2)+\cdots. \tag{12}$$

This is a significant simplification because the problem has been reduced to finding the spring potential energy for only dumbbell models.

The spring force law is calculated by first determining the constant extension partition function given in Eq. (3) or alternatively in Eq. (10). The result is proportional to the well-known probability density of a three-dimensional random walk given by Rayleigh's formula [Rayleigh (1919)] or Treloar's formula [Treloar (1975)]. Using Rayleigh's integral form, the partition function is

$$\Omega(\mathbf{r})\propto\frac{1}{r}\int_0^\infty u\sin(ur)\left[\frac{\sin(uA)}{uA}\right]^\nu du, \tag{13}$$

where $r=|\mathbf{r}|$, A is the Kuhn length, ℓ is the fully extended length of a spring, and $\nu=\ell/A$ is the number of Kuhn lengths represented by each spring. Alternatively, the partition function can be written as Treloar's summation formula as

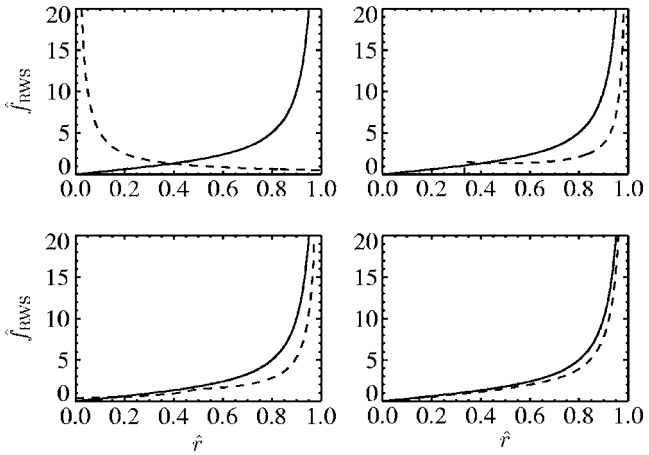

FIG. 3. Comparison of spring force laws of the random walk spring model (dashed line) with the inverse Langevin function (solid line). The dimensionless axes are $\hat{f}_{\mathrm{RWS}}=f_{\mathrm{RWS}}A/(k_BT)$ and $\hat{r}=r/\ell$. The results are for $\nu=2$ (upper left), $\nu=3$ (upper right), $\nu=4$ (lower left), and $\nu=8$ (lower right).

$$\Omega(\mathbf{r}) \propto \frac{1}{r}\sum_{t=0}^{\tau} \frac{(-1)^t}{t\,!\,(\nu-t)!}\left[\frac{\nu-(r/A)-2t}{2}\right]^{\nu-2}, \tag{14}$$

where the upper limit τ is taken from the condition

$$(\nu-r/A)/2-1 \leqslant \tau < (\nu-r/A)/2. \tag{15}$$

The spring potential energy to within an arbitrary additive constant is found using Eq. (5) to be

$$U_s(\mathbf{r}) = -k_BT \ln\left\{\frac{1}{r}\int_0^{\infty} u\sin(ur)\left[\frac{\sin(uA)}{uA}\right]^{\nu} du\right\}. \tag{16}$$

The spring force is calculated as the derivative of the potential energy where by convention a positive value is a retractive force. Recall that this set of spring force laws *exactly* reproduces the behavior of the FJC for integer ν, while in current simulations the inverse Langevin function, or some approximation to it, is being used for all ν. In Fig. 3 we compare the force laws from the RWS model with the inverse Langevin function for different values of ν.

The first case to consider is $\nu=1$. One important property of a coarse-graining method is that if the level of coarse-graining is reduced to the level of the detailed model, the result of the "coarse-graining" is the same as the detailed model. The probability of a random walk after a single step is a delta function, which is reproduced by Eq. (13). One way of getting a spring with a delta function distribution is to use an infinitely stiff Fraenkel spring.

We see that for small ν the RWS model has special features that are not conventionally seen in bead-spring chain models. Note that these features are *necessary* in order for the model to have the correct behavior. When $\nu=2$ the RWS model spring force increases with decreasing extension, diverging at zero extension. There is also a discontinuous divergence at full extension. The functional form is given by

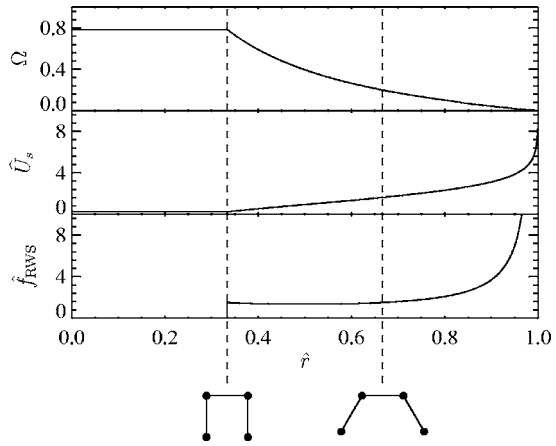

FIG. 4. Progression from the constant extension partition function to the spring force in the random walk spring model for $\nu=3$. The dimensionless axes are $\hat{U}_s=U_s/(k_BT)$, $\hat{f}_{\mathrm{RWS}}=f_{\mathrm{RWS}}A/(k_BT)$ and $\hat{r}=r/\ell$. Sample configurations are shown for the three rod system at fractional extensions of $\hat{r}=1/3$ and $\hat{r}=2/3$.

$$f_{\mathrm{RWS}}(r;\nu=2)=\frac{k_BT}{r},\quad r<\ell. \tag{17}$$

For $\nu=3$ the force law is zero below one-third extension, at which point there is a jump discontinuity. Above one-third extension the spring force is

$$f_{\mathrm{RWS}}(r;\nu=3)=\frac{3k_BTA}{(3A-r)r},\quad \ell/3<r<\ell. \tag{18}$$

For $\nu=4$ the force has a nonzero limit at zero extension and a discontinuous first derivative at half extension

$$f_{\mathrm{RWS}}(r;\nu=4)=\frac{3k_BT}{8A-3r},\quad 0<r<\ell/2, \tag{19}$$

$$f_{\mathrm{RWS}}(r;\nu=4)=\frac{k_BT(4A+r)}{(4A-r)r},\quad \ell/2<r<\ell. \tag{20}$$

The dramatic changes in the form of the force law come about when the true polymer takes configurations of a certain form. They also correspond to changes in the upper limit τ in Treloar's formula, Eq. (15). To better illustrate this, in Fig. 4 we show $\Omega, U_s, f_{\mathrm{RWS}}$, and sample configurations for $\nu=3$. We see that the step discontinuity occurs when the ends are separated by a distance equal to one rod. For end-to-end distances less than one rod, the partition function (number of configurations) is constant, resulting in a vanishing force. Beyond this special point the partition function decreases but with a discontinuous slope. This change in slope causes a jump discontinuity in the force. The change is discontinuous because the rods are stiff. If one were to coarse-grain three Fraenkel springs into a single spring, it would be continuous, with the discontinuity appearing when the Fraenkel springs become infinitely stiff.

B. Unequal rod lengths

The freely jointed chain discussed thus far consists of rods of equal length. We can examine how sensitive the spring potentials are to a distribution of rod lengths, which would correspond roughly to a polymer with regions of differing flexibility. If the scale over which the flexibility changes is larger than the Kuhn length, a freely jointed chain with changing rod lengths should be a reasonable model. This situation could appear in block copolymers, atactic polymers, and DNA having blocks with the same repeated base pair. We first must discuss the behavior of the system that is to be modeled. For the equal rod case, the constant force response is the Langevin function for any number of rods. However, the behavior of a general chain is a sum over the response of each rod

$$\langle z\rangle = \sum_{i=1}^{N_r} \langle z_i\rangle = \sum_{i=1}^{N_r} A_i \mathcal{L}\left(\frac{fA_i}{k_{\mathrm{B}}T}\right), \tag{21}$$

where i denotes the different rods in the chain which is to be modeled by a spring, N_r is the number of rods, A_i is the length of rod i, and $\mathcal{L}$ is the Langevin function. In general, this summation does not simplify. To understand how this response differs from the response with equal lengths, we examine the small and large force limits and try to identify an effective Kuhn length for which this appears like a single Langevin function.

If we examine the limit when f is large compared to k_BT/A_i even for the smallest A_i, the average fractional extension of the chain becomes

$$\frac{\langle z\rangle}{\ell} \simeq 1 - \frac{k_BTN_r}{f\ell}, \tag{22}$$

where ℓ is the fully extended length of spring and is equal to the sum of the rod lengths

$$\ell = \sum_{i=1}^{N_r} A_i. \tag{23}$$

Comparing this behavior with a system with equal rod lengths gives a high-force effective Kuhn length

$$A_{\mathrm{eff,h}} = \frac{\ell}{N_r} = \frac{1}{N_r}\sum_{i=1}^{N_r} A_i = \bar{A}. \tag{24}$$

We have introduced the overbar notation for the average over the rods in the chain. If we expand the fractional extension for small force, the behavior becomes

$$\frac{\langle z\rangle}{\ell} \simeq \frac{f}{3k_BT}\sum_{i=1}^{N_r} A_i^2/\ell. \tag{25}$$

Therefore the low-force effective Kuhn length is

$$A_{\mathrm{eff,l}} = \sum_{i=1}^{N_r} A_i^2/\ell = \sum_{i=1}^{N_r} A_i^2 / \sum_{i=1}^{N_r} A_i = \overline{A^2}/\bar{A}. \tag{26}$$

The high-force value is simply the average rod length, while the low-force value in Eq. (26) is larger. The larger the spread in rod lengths, the larger the difference between the two.

After understanding the constant force response of the bead-rod chain, we can examine the spring force needed in a bead-spring model that gives the same constant force

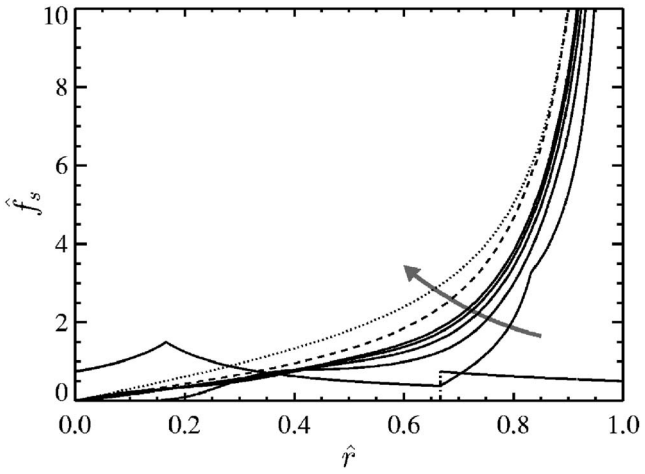

FIG. 5. Series of spring forces necessary to model chains with m rods of length A and m rods of length $5A$ for $m=1, 2, 3, 4, 5, 6$, with the arrow denoting increasing m. The dimensionless axes are $\hat{f}_s=f_s 3A/k_BT$ and $\hat{r}=r/\ell$. The dashed line corresponds to $m=\infty$. The dotted line is the inverse Langevin function. Note that the $m=1$ force law diverges at $\hat{r}=2/3$ and $\hat{r}=1$.

response (which itself differs from a single Langevin function). As shown previously, this spring force comes from the constant extension response of the bead-rod chain. This can be written again using Rayleigh's formula but for a random walk with nonidentical steps. For example, to use a spring to model a three rod system with rod lengths A_1, A_2, and A_3 one should use a spring potential energy of

$$U_s(\mathbf{r}) = -k_BT \ln\left[\frac{1}{r}\int_0^\infty u \sin(ur)\frac{\sin(uA_1)}{uA_1}\frac{\sin(uA_2)}{uA_2}\frac{\sin(uA_3)}{uA_3}du\right]. \tag{27}$$

The spring force is the derivative of this potential.

Let us examine a specific system to illustrate the behavior of these unequal rod chains. Figure 5 shows the spring force needed for a series of chains each with m rods of length A and m rods of length $5A$ for m ranging from 1 to 6. Similar to the equal rod case, for short chains (small m) the spring force laws needed have discontinuities. For example, when $m=1$ it is impossible for the fractional extension to be less than $2/3$. Because a positive force is a retractive force, the force diverges to $-\infty$ to prevent the fractional extension from being less than $2/3$. Only in the large m limit does the spring force-law approach the constant force behavior. Note that even in this limit the spring force needed differs from a single Langevin function based on the average rod length.

Figure 5 allowed us to examine how the chains approach the infinitely long limit if the rods have a significant difference in lengths. To further examine how different rod lengths affect the spring force law needed to model the chain, we will compare chains will the same contour length but with different ratios of rod lengths. The system contains m rods of length A and m rods of length pA. The constraint of constant contour length means that $m(1+p)$ is held constant. Figure 6 shows an example of the rod system with $m(1+p)=12$ and m ranging from 1 to 6. Note that the $m=2$ case was already seen in Fig. 5, and the $m=6$ case has 12 equal length rods. For this example, two effects help make the response closer to the inverse Langevin function as m increases; not only does the number of rods increase with m but also the variance in rod lengths decreases.

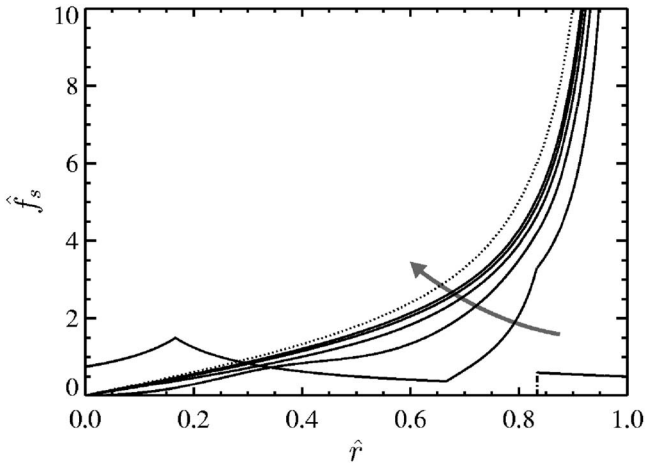

FIG. 6. Series of spring forces necessary to model chains with m rods of length A and m rods of length pA for $m=1, 2, 3, 4, 5, 6$, with the arrow denoting increasing m. The value of p is determined from the condition of constant contour length, $m(1+p)=12$. The dimensionless axes are $\hat{f}_s=f_s(6/m)A/k_BT$ and $\hat{r}=r/\ell$. The dotted line is the inverse Langevin function. Note that the $m=1$ force law diverges at $\hat{r}=5/6$ and $\hat{r}=1$.

In Fig. 6 we scaled the force using the average rod length, which changes with m. We saw that for the constant force response this scaling made curves for all distributions of rod lengths and number of rods have the same high force limiting behavior. Let us examine closer the constant extension response near full extension. Consider a chain of ν rods with lengths A_1, A_2, to A_ν. We denote the smallest rod length by A_s. It has been observed that in the region $\ell - 2A_s < r < \ell$ the partition function is

$$\Omega(\mathbf{r}) \propto \frac{(\ell - r)^{\nu-2}}{r}. \tag{28}$$

This has been explicitly verified for a number of examples for small ν, while a general proof for arbitrary ν appears excessively tedious like a related proof given in Appendix F of Flory (1989). The spring force needed in this region of extension is

$$f_s(r) = k_B T\left(\frac{1}{r} + \frac{\nu-2}{\ell - r}\right). \tag{29}$$

If we nondimensionalize the force using the average Kuhn length, $\bar{A}$, the force as a function of fractional extension, $\hat{r}$, is

$$\frac{f_s\bar{A}}{k_BT} = \frac{1 + (\nu-3)\hat{r}}{\nu\hat{r}(1-\hat{r})}. \tag{30}$$

Because this force only depends on ν and not the exact distribution of rod lengths, the force is the same in this region as an equal rod system having ν rods each of length $\bar{A}$. Note that this relation is *exact* over a *finite* range which is determined by the smallest rod length. This can be compared with the constant force response, for which it only matches the response of ν rods each of length $\bar{A}$ in the *limit* $r \to \ell$.

By examining the FJC with unequal rod lengths, we have examined a crude model for chains with variable flexibility. Both the constant force response and the constant extension response differ from the equal rod case (a single Langevin function). In other words,

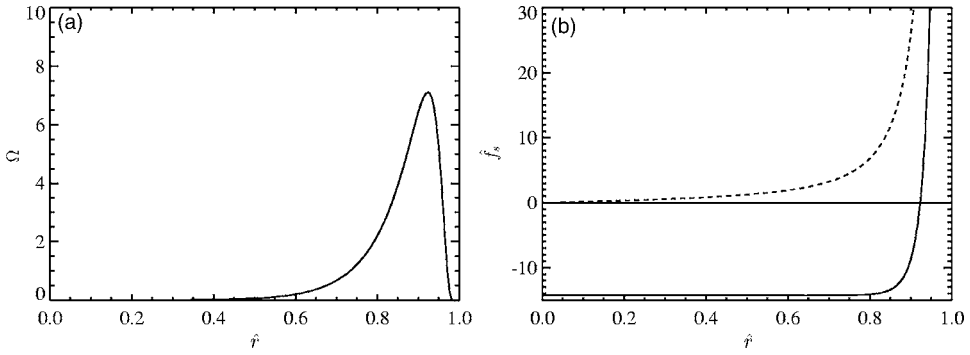

FIG. 7. (a) Constant extension partition function of a single F-actin filament. (b) Comparison of the spring force law determined by the PET method (solid line) for a dumbbell model of an F-actin filament with the Marko-Siggia interpolation formula (dashed line). The force is made dimensionless using the persistence length, $\hat{f}_s = f_s A_p / k_B T$.

even in the infinite chain limit, the unequal rod system *can* be distinguished from an equal rod model. Also, throughout the analysis, the order of the rods within a spring did not matter. This can be seen directly from Eq. (27) for the three rod system. The formula is the same independent of the ordering of the rods.

C. Worm-like chain

The next polymer model we examine is the worm-like chain (WLC), but initially only for dumbbell models. The next section discusses the extension to multispring chains. The application for a dumbbell follows the general prescription given in Eq. (5). If the worm-like chain contains a large number of persistence lengths, then the spring force law reduces to the long chain limit approximated by the Marko-Siggia interpolation formula. However, many biopolymers of interest, such as F-actin and microtubules, do not contain many persistence lengths. In contrast to the FJC, for which exact analytical results can be obtained for short chains, the analytical calculation of the exact distribution function for short WLCs cannot be done at this time. However, a number of numerical and approximate analytical techniques have been developed recently [Wilhelm and Frey (1996); Dhar and Chaudhuri (2002); Samuel and Sinha (2002)].

As an example, we calculate the spring force needed to model a single actin filament using a dumbbell. Because the end-to-end distance distribution for an actin filament has been measured experimentally [Le Goff *et al.* (2002)], this example illustrates how the use of the distribution function to produce a bead-spring model is not restricted to analytical models. The distribution function can come directly from experiments.

Le Goff *et al.* (2002) show that the distribution for actin matches well to the worm-like chain, and Wilhelm and Frey (1996) develop a good approximation to that behavior. In Fig. 7(a) we show the distribution function of a three-dimensional WLC calculated from the approximate formula given by Wilhelm and Frey (1996) for the actin parameters found by Le Goff *et al.* (2002): $L = 13.40\ \mu$m, $A_p = 16.1\ \mu$m. In Fig. 7(b) we compare the resulting spring force necessary to reproduce the actin distribution with the Marko and Siggia interpolation formula. The dramatic difference between the force laws illustrates the importance of choosing the correct one, because the incorrect use of the Marko and Siggia form would result in significant errors.

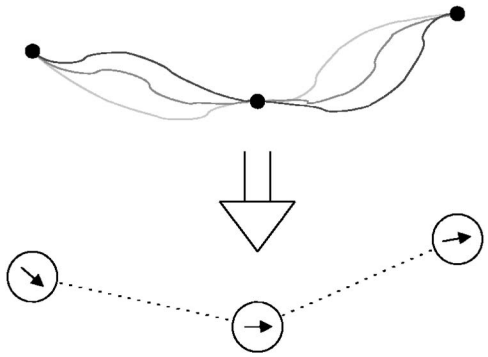

FIG. 8. Restricting the configurations within a category eliminates the coupling in a multispring worm-like chain model. Within each category the reference points (black circles) are held fixed as well as the polymer's tangent vector at the reference point. The lines signify different polymer configurations within the category. The coarse-grained model consists of beads which have a vector direction which is the direction of the polymer's tangent vector. The interaction of neighboring beads depends both on the bead positions and the bead directions.

D. Multispring worm-like chain models

In order to develop a multispring model of the worm-like chain, one must calculate the multidimensional partition function $\Omega(\mathbf{r}_1,\mathbf{r}_2,\ldots)$. This illustrates a hurdle with implementing the PET method. For models such as the worm-like chain with coupling across the reference points (black circles in Fig. 2), the multidimensional partition function is not separable, and therefore the spring potential energy is not separable into a sum over each spring.

However, we can use the same thought process used in Fig. 2 to overcome the difficulty in a systematic way. We can eliminate the coupling between the segments by further restricting the category of configurations. The new type of model is illustrated in Fig. 8. In addition to holding points along the polymer with fixed positions, the tangent vector of the polymer is held fixed at each of these points. Because the tangent vector is held fixed, there is no coupling across the points. We can replace the category of configurations by a single configuration of a coarse grained model. This new coarse grained model is not a typical type of bead-spring chain, but a series of beads that have a direction associated with them (the direction of the polymer's tangent vector). The interaction of two neighboring beads depends both on the vector connecting the bead centers, $\mathbf{r}$, and the tangent vectors associated with the beads, $\mathbf{t}_1$ and $\mathbf{t}_2$. The "potential energy" of this interaction is

$$U(\mathbf{r},\mathbf{t}_1,\mathbf{t}_2) = -k_BT \ln \Omega(\mathbf{r},\mathbf{t}_1,\mathbf{t}_2), \tag{31}$$

where $\Omega(\mathbf{r},\mathbf{t}_1,\mathbf{t}_2)$ is the partition function in the ensemble where both the separation of the ends and tangent vectors at the ends are held fixed.

While this new type of coarse grained model will give the correct equilibrium distribution function as the worm-like chain at any level of discretization, it may not be computationally desirable to perform simulations such as Brownian dynamics (BD) with such a model.

We propose that this system can be approximated by a conventional bead-spring chain with bending potentials. The spring force in this approximation would be taken as the force in a dumbbell model of the short segment of polymer. This separation is a reasonable first approximation because it correctly models the behavior at the two extremes of discretization.

In the limit of a large number of persistence lengths between reference points, the coupling vanishes and thus the bending energy should vanish. In the limit of zero persistence lengths between reference points, the polymer acts like a rigid rod. The polymer model of rigid rods with bending potentials is the Kratky-Porod model if we choose the bending potential to be

$$U_{\text{bend}}(\theta) = \frac{k_B T A_p}{2\ell}\theta^2, \tag{32}$$

where θ is the angle between the directions of successive rods, ℓ is the length of the rod, and A_p is the persistence length. In the limit of ℓ much smaller than A_p this approaches the continuous WLC model. This bending energy could also be used when the spring length, ℓ, is much larger than the persistence length, A_p, because it correctly vanishes in that limit. We leave a detailed analysis of the decomposition approximation using bending energy and an analysis of how the bending energy varies with $\nu=\ell/A$ for future work.

E. Rheology of the models

The force laws presented give the same equilibrium behavior as the polymer including force-extension behavior in both the constant force and constant extension ensembles. Therefore it is natural to use these bead-spring chains to model the polymer behavior in other situations such as in flow. We have previously derived the zero-shear properties of bead-spring chains for arbitrary force law [Underhill and Doyle (2004)]. We can use those results to analyze the rheological properties of these bead-spring chains.

In Underhill and Doyle (2004) it is shown that the retarded motion expansion coefficients, which describe the rheological response in slow and slowly changing flows, can be written in terms of the force-extension behavior. Note that the analysis is for dilute polymer solutions and excluded volume and hydrodynamic interactions are not included. There are no bending potentials allowed and the spring force law must be the same for each spring. The first two retarded motion coefficients, b_1 and b_2, are

$$b_1 - \eta_s = \eta_{0,p} = \left[\frac{n_p(N\zeta)LA}{12}\right]\left(\frac{N+1}{N}\right)\left(\lim_{\hat{f}\to 0}\frac{\partial}{\partial \hat{f}}\langle \hat{z}_{\text{tot}}\rangle_m\right), \tag{33}$$

$$b_2 = \frac{-\Psi_{1,0}}{2} = \left[\frac{-n_p(N\zeta)^2L^2A^2}{120k_BT}\right]\left\{\left(\frac{1}{3\alpha}\lim_{\hat{f}\to 0}\frac{\partial^3}{\partial \hat{f}^3}\langle \hat{z}_{\text{tot}}\rangle_{\text{m}}\right)\left[\frac{(N^2+1)(N+1)}{N^3}\right] + \left(\lim_{\hat{f}\to 0}\frac{\partial}{\partial \hat{f}}\langle \hat{z}_{\text{tot}}\rangle_{\text{m}}\right)^2\left[\frac{(N+1)(2N^2+7)}{6N^2(N-1)}\right]\right\}. \tag{34}$$

The values of b_1 and b_2 are related to the viscosity of the Newtonian solvent, η_s, the polymer contribution to the zero-shear viscosity, $\eta_{0,p}$, and the zero-shear first normal stress coefficient, $-\Psi_{1,0}$. The parameters in the response are the number density of polymers, n_p, the number of beads, N, the drag coefficient on a bead, ζ, the polymer contour length, L, a length proportional to the Kuhn length or persistence length, A, and the ratio of the contour length to A, $\alpha=L/A$. The influence of the spring force law enters through the derivatives with respect to force of the average extension in the limit of zero force. The average z extension of the model has been made dimensionless using the contour length L, and the force has been made dimensionless using k_BT/A. In general, the derivatives of the force-extension behavior can be a function of $\nu=\ell/A$.

The terms other than the force-extension behavior are contributed to the fact that the hydrodynamic drag is exerted only on the beads and not along the continuous polymer contour. When the number of beads is large enough, these factors disappear. When using spring force laws such as FENE or Marko-Siggia, the force-extension terms change when each spring represents a small segment of polymer. This causes significant errors in the rheology which places a limit on how small the springs can be [Underhill and Doyle (2004)]. Using the spring laws discussed here eliminates this error. For example, for the RWS model discussed in Sec. III A and choosing A to be the Kuhn length in nondimensionalizing the force, the bead-spring chain always has

$$\lim_{\hat{f}\to 0}\frac{\partial}{\partial \hat{f}}\langle \hat{z}_{\mathrm{tot}}\rangle_m = \frac{1}{3} \tag{35}$$

$$\lim_{\hat{f}\to 0}\frac{\partial^3}{\partial \hat{f}^3}\langle \hat{z}_{\mathrm{tot}}\rangle_m = \frac{-2}{15}. \tag{36}$$

We can also use the retarded motion coefficients to gauge the difference between the different dumbbell models of F-actin shown in Fig. 7(b). For a dumbbell model, it is useful to write b_1 and b_2 directly in terms of the equilibrium averages of the spring length. These moments of the spring length are equal to

$$\langle \hat{r}^n\rangle_{\mathrm{eq}} = \frac{\int_0^1 d\hat{r}\ \hat{r}^{n+2}\exp[-U(\hat{r})/(k_{\mathrm{B}}T)]}{\int_0^1 d\hat{r}\ \hat{r}^2\exp[-U(\hat{r})/(k_{\mathrm{B}}T)]}, \tag{37}$$

where U is the spring potential energy. For the dumbbell models, writing b_1 and b_2 in terms of these moments of the spring length gives

$$b_1 - \eta_s = \eta_{0,p} = \left(\frac{n_p\zeta L^2}{12}\right)\langle \hat{r}^2\rangle_{\mathrm{eq}}, \tag{38}$$

$$b_2 = \frac{-\Psi_{1,0}}{2} = \left(\frac{-n_p\zeta^2 L^4}{240 k_B T}\right)\langle \hat{r}^4\rangle_{\mathrm{eq}}. \tag{39}$$

The force laws in Fig. 7(b) will have different equilibrium averages. The averages for the Marko-Siggia spring can be calculated using numerical integration. Using the Marko-Siggia dumbbell to model an F-actin filament with the contour length and persistence length from Sec. III C, the averages are $\langle \hat{r}^2\rangle_{\mathrm{eq}}=0.41$ and $\langle \hat{r}^4\rangle_{\mathrm{eq}}=0.21$. Alternatively, using the dumbbell model that correctly models the worm-like chain distribution has averages $\langle \hat{r}^2\rangle_{\mathrm{eq}}=0.77$ and $\langle \hat{r}^4\rangle_{\mathrm{eq}}=0.61$. This means that the spring force laws in Fig. 7(b) have a factor of 2 different $\eta_{0,p}$ and a factor of 3 different b_2.

F. Practical implementation of the models

While the models developed using the constant extension ensemble are advantageous in that they give the correct equilibrium behavior and provide a systematic method for changing levels of coarse-graining, some practical issues remain for using them in computations such as Brownian dynamics simulations. For small numbers of rods per spring,

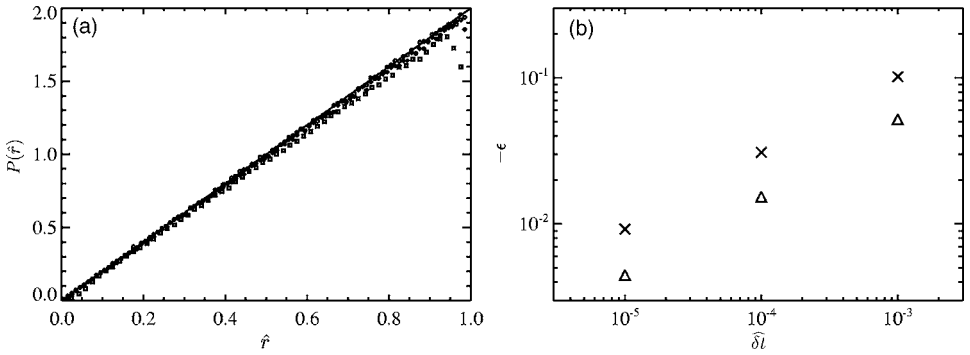

FIG. 9. This shows the convergence of a BD simulation for a spring force law that models two rods of a freely jointed chain. (a) Histogram of the probability density of the spring length from a BD simulation compared with the exact distribution. The time steps used were $\widehat{\delta t}=10^{-3}$ (□), $\widehat{\delta t}=10^{-4}$ (◇), and $\widehat{\delta t}=10^{-5}$ (○). (b) The relative error in the second moment $\langle \hat{r}^2 \rangle_{\text{eq}}$ (△) and the fourth moment $\langle \hat{r}^4 \rangle_{\text{eq}}$ (×) from the BD simulations.

the spring force laws can have discontinuities. How do discontinuous force laws perform in BD simulations? We address this question by simulating directly using BD the two-rod and three-rod spring force laws at equilibrium.

The two-rod spring force law is proportional to r^{-1} for allowable extensions. At full extension, the retractive force must jump to $+\infty$ to prevent the spring from extending past that point. The two features not common to spring force laws are the divergence at small extension and the discontinuity at full extension. To test the ability to use this force law in a Brownian dynamics simulation, we use a simple explicit Euler integration scheme [Öttinger (1996)]. With this scheme it is possible for the length of the spring at the end of a time step to be larger than the fully extended length of the spring. This is analogous to two hard spheres which are not allowed to have a separation distance smaller than their diameter. For this spring force law, we implement the same type of algorithm used for hard spheres [Heyes and Melrose (1993); Foss and Brady (2000)]. If the spring is past full extension at the end of a time step, we rescale the length of the spring to be at full extension. This algorithm is known to converge to the correct answer as the time step is reduced. For larger time steps, it is known that this algorithm produces a delta function in the probability density at full extension with a corresponding depletion at smaller extensions.

We tested the algorithm by choosing a random starting configuration and stepping forward in time to equilibrate in a stagnant solvent. We then continued simulating at equilibrium and sampling the magnitude of the extension of the spring. From this we build a histogram of the probability distribution of the spring length. The spring length was sampled 10^6 times to reduce the statistical error from finite sampling so most of the error is due to the nonzero time step. We show in Fig. 9(a) the histograms for different time steps compared to the true distribution. The time step is nondimensionalized as

$$\widehat{\delta t} \equiv \delta t\left(\frac{k_B T}{\zeta \ell^2}\right), \tag{40}$$

where ζ is the drag coefficient on a bead and ℓ is the fully extended length of the spring. We also show in Fig. 9(b) the convergence of the second and fourth moments of the spring length, $\langle \hat{r}^2 \rangle_{\text{eq}}$ and $\langle \hat{r}^4 \rangle_{\text{eq}}$, to the true values. To avoid ambiguity in the sign, we define the relative error as

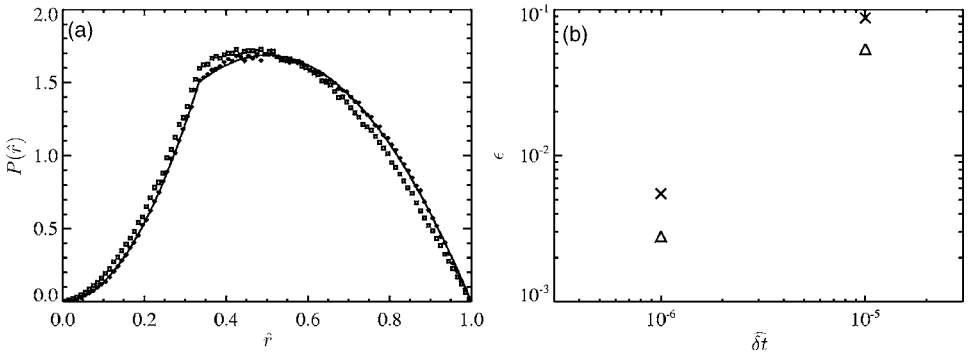

FIG. 10. This shows the convergence of a BD simulation for a spring force law that models three rods of a freely jointed chain. (a) Histogram of the probability density of the spring length from a BD simulation compared with the exact distribution. The time steps used were $\widehat{\delta t}=10^{-5}$ (□) and $\widehat{\delta t}=10^{-6}$ (◇). (b) The relative error in the second moment $\langle \hat{r}^2 \rangle_{\text{eq}}$ (△) and the fourth moment $\langle \hat{r}^4 \rangle_{\text{eq}}$ (×) from the BD simulations.

$$\epsilon \equiv \frac{\text{true value} - \text{calculated value}}{\text{true value}}. \tag{41}$$

The three-rod spring force law also has a feature not common to force laws. It has a finite jump in the force at 1/3 extension. This jump is equivalent to a discontinuous slope in the probability density. We again test the ability of a simple explicit Euler scheme to capture this feature. Even though the spring force law does continuously diverge at full extension, with this scheme it is possible to end a time step past full extension. While there exist more sophisticated schemes for handling this, we opt for the simple algorithm of rescaling the spring to be at 0.99999 of full extension.

We formed the probability density histogram in the same way as for the two-rod spring. In Fig. 10(a) the histograms for different time steps are compared to the true distribution. We also show in Fig. 10(b) the convergence of the second and fourth moments of the spring length to the true values.

These two examples show that it is possible to simulate the new spring force laws using simple BD algorithms. More elaborate schemes may be able to increase the size of time steps although at the increased computation cost of a more sophisticated algorithm.

The other main practical issue concerns the spring laws when each spring represents a larger number of springs. Although we have shown that the spring force from the RWS model [calculated from Eq. (16)] exactly represents the freely jointed chain, and similarly for the unequal rod case, the analytical expressions for the spring force laws become increasing complicated as each spring represents more rods. We have seen that the spring force law has different forms in different regions of fractional extension. For the equal rod length case the number of different regions is 1/2 of the number of rods per spring (rounding up to the nearest integer). Thus as the number of rods per spring increases, the number of different regions increases dramatically. Within each of these regions, the force law is a rational function where the degree of the polynomials typically increases rapidly as the number of rods per spring increases. The large number of regions and the complexity within each region decreases the practicality of these force laws for large number of rods per spring. However, in this limit the spring force laws are becoming smooth, making it likely that approximate force laws can be developed in the same spirit as approximating the inverse Langevin function by a simple rational function.

Our task for the remainder of this section is to develop a spring force law which approximates the RWS model, because it is that spring force law that exactly models the freely jointed chain. We start by considering the equal rod case. We have shown that the RWS model can be used directly when each spring represents two or three rods. When each spring represents four rods, the RWS model only has two regions of extension, with a simple form in each region, and so could also be easily implemented in BD simulations.

For the cases where each spring represents five or six rods the spring force laws have three regions in extension. The force law in the third region (near full extension) is given by Eq. (30). We can develop a single functional form that can approximate the first two regions. In this way we can approximate the RWS model which has three regions in extension by a spring force law which only has two regions and so is easier to implement in simulations. An approximate force law for the five-rod case is

$$\frac{f_s A}{k_B T} \approx \frac{539\hat{r}/225}{1 - 3\hat{r}^2/5}, \quad 0 < \hat{r} < 3/5, \tag{42}$$

$$\frac{f_s A}{k_B T} = \frac{1 + 2\hat{r}}{5\hat{r}(1 - \hat{r})}, \quad 3/5 < \hat{r} < 1. \tag{43}$$

The parameters for the force law in the first region were chosen by first assuming a functional form in $\hat{r}$ with two adjustable constants. The parameters were constrained so that the force law is continuous at $\hat{r}=3/5$ because the RWS model for five rods is continuous. The other free parameter was chosen to give a small error in the second and fourth moment of the spring length at equilibrium. The error in $\langle \hat{r}^2 \rangle_{\text{eq}}$ by using this approximate force law to model five rods is 0.02%. The error in $\langle \hat{r}^4 \rangle_{\text{eq}}$ is 0.0006%.

A similar method can be used to approximate the six-rod case. The approximate force law is

$$\frac{f_s A}{k_B T} \approx \frac{63\hat{r}/25 - 49\hat{r}^3/125}{1 - 9263\hat{r}^2/13500}, \quad 0 < \hat{r} < 2/3, \tag{44}$$

$$\frac{f_s A}{k_B T} = \frac{1 + 3\hat{r}}{6\hat{r}(1 - \hat{r})}, \quad 2/3 < \hat{r} < 1. \tag{45}$$

This approximate force law for the six-rod system has an error of 0.01% in $\langle \hat{r}^2 \rangle_{\text{eq}}$ and an error of 0.02% in $\langle \hat{r}^4 \rangle_{\text{eq}}$.

The advantage of still using two regions for the five- and six-rod cases is that we can utilize exactly the RWS model in the final region of extension. This allows us to build an approximation that accurately represents many properties such as the second and fourth moments of the spring length and also the response under large stretching.

For even larger number of rods per spring the final region near full extension which has a simple force law is only valid over a smaller and smaller region of extension. In this case the advantage to using two spring force laws spliced together does not seem great and so we have chosen to develop a single approximate force law over the entire extension range. While many possible forms are possible to approximate the true spring force laws, we choose the form

$$\frac{f_s A}{k_B T} = \frac{C\hat{r} + D\hat{r}^3}{1 - \hat{r}^2}, \tag{46}$$

where A is the rod length and C and D do not depend on the fractional extension, $\hat{r}$, but will depend on the number of rods represented by the spring, ν. The dependence on $\hat{r}$ takes the same form as the Cohen force law [Cohen (1991)]. We will see that with an appropriate choice of C and D, this can give an accurate representation of the freely jointed chain. Because we have chosen the same form in $\hat{r}$ as the Cohen force law, calculations such as BD simulations can be easily and quickly modified to use the new force law with no loss of computation speed but a uniformly more accurate result.

Although we are not using the RWS force law near full extension, we will still require that the limiting behavior of our approximate form match the limiting behavior of the RWS force law. The result of this choice will be that the approximate spring will behave like the freely jointed chain in the limit of strong stretching. As the fractional extension approaches 1, the RWS force law diverges as

$$\frac{f_s A}{k_B T} \to \frac{1 - 2/\nu}{1 - \hat{r}}. \tag{47}$$

For our approximate force law to diverge in the same manner, we obtain the constraint on C and D of

$$C + D = 2 - 4/\nu. \tag{48}$$

We must now develop a method for determining the remaining free parameter. One natural method would be to examine the RWS force law at small extension, find the coefficient to $\hat{r}$ in that expansion which will be a function of ν, and match this coefficient with C. Because the constraint on $C+D$ is to capture the strong stretching limit, the rationale behind this choice would likely be so that the spring correctly captures the equilibrium limit. However, with this choice the second moment of the spring length at equilibrium, $\langle \hat{r}^2 \rangle_{\text{eq}}$, is *not* correct. This is because, even at equilibrium, the spring samples the nonlinear regions of the force law, and the shape of the approximate force law does not exactly capture the shape of the RWS model.

Alternatively, one could calculate numerically the function $C(\nu)$ such that the second moment of the spring length for the approximate force law matches exactly the freely jointed chain (which is also the same as the RWS model). Recall that the second moment of the spring length is a key property that is important to capture [Underhill and Doyle (2004)]. Not only is it related to the size of the coil at equilibrium, but also it is related to the zero-shear viscosity. In the constant force ensemble, the slope of the average extension versus force curve at small force is also proportional to the second moment of the spring length.

Instead of having to deal with a numerical function $C(\nu)$, it would be better to have a simple approximate formula for $C(\nu)$ that still gives a very small error in the second moment of the spring length. Another reason an approximate form for $C(\nu)$ is sufficient is that even if we could make the error in the second moment vanish, the shape of the spring force law will limit the ability to capture other properties like the fourth moment exactly.

Using the asymptotic expansion developed in Underhill and Doyle (2004), the second moment of the spring length for the force law [Eq. (46)] with the constraint in Eq. (48) is

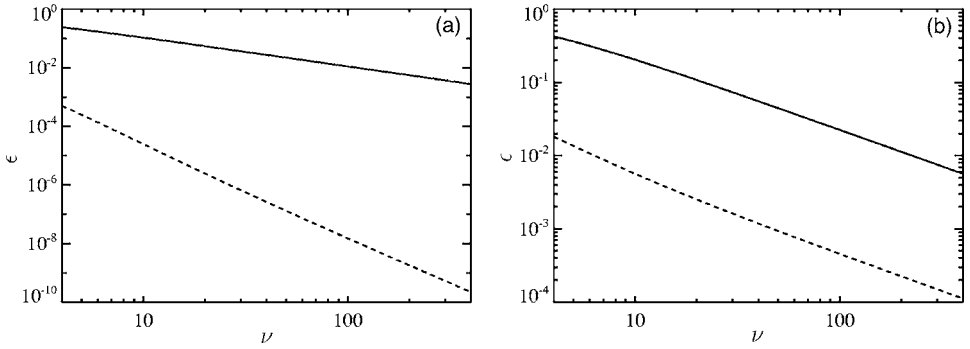

FIG. 11. Relative error in the equilibrium moments of the spring length between an approximate spring force law compared with an equal rod freely jointed chain. The solid lines are for the Cohen force law, and the dashed lines are for the new force law [Eq. (52)]. (a) Relative error in the second moment, $\langle \hat{r}^2 \rangle_{\text{eq}}$. (b) Relative error in the fourth moment, $\langle \hat{r}^4 \rangle_{\text{eq}}$.

$$\langle \hat{r}^2 \rangle_{\text{eq}} \sim \frac{3}{\nu C} - \frac{30}{\nu^2 C^3} + \frac{30(24 - 7C + 2C^2)}{\nu^3 C^5} + \mathcal{O}\left(\frac{1}{\nu^4}\right). \tag{49}$$

We want to choose $C(\nu)$ such that this second moment is the same as the freely jointed chain. The freely jointed chain has $\langle \hat{r}^2 \rangle_{\text{eq}} = 1/\nu$. By choosing

$$C = 3 - \frac{10}{3\nu} + \frac{10}{27\nu^2}, \tag{50}$$

the second moment of the spring length for the approximate spring force law [Eq. (46)] is

$$\langle \hat{r}^2 \rangle_{\text{eq}} \sim \frac{1}{\nu} + \mathcal{O}\left(\frac{1}{\nu^4}\right). \tag{51}$$

The resulting approximate spring force law is

$$\frac{f_s A}{k_B T} = \frac{\left(3 - \frac{10}{3\nu} + \frac{10}{27\nu^2}\right)\hat{r} - \left(1 + \frac{2}{3\nu} + \frac{10}{27\nu^2}\right)\hat{r}^3}{1 - \hat{r}^2}. \tag{52}$$

To quantify the accuracy of this approximate spring force law, we need to compare it's properties with those of the underlying freely jointed chain. The average $\langle \hat{r}^2 \rangle_{\text{eq}}$ of this spring force law is compared in Fig. 11(a) to the freely jointed chain it is meant to represent as a function of the number of rods per spring. From the asymptotic expansion of the second moment, Eq. (51), we see that the relative error should go like ν^{-3} which we see explicitly from Fig. 11(a). The approximate spring force law has an error of 0.01% at $\nu = 6$ and smaller error for larger ν. For reference we show the error if the Cohen force law were used. An asymptotic expansion of the second moment of the spring length using the Cohen force law shows the relative error decays like ν^{-1} as seen in the figure. The slight changes made to the Cohen form have had a significant impact. The error has been reduced by over a factor of 1000. The new force law can even be used down to four rods per spring with only a small error.

The fourth moment of the spring length is also important to capture correctly because of it's impact on zero-shear rheology. Similar to the second moment, we show in Fig. 11(b) the error in the fourth moment of the spring length for the approximate force law

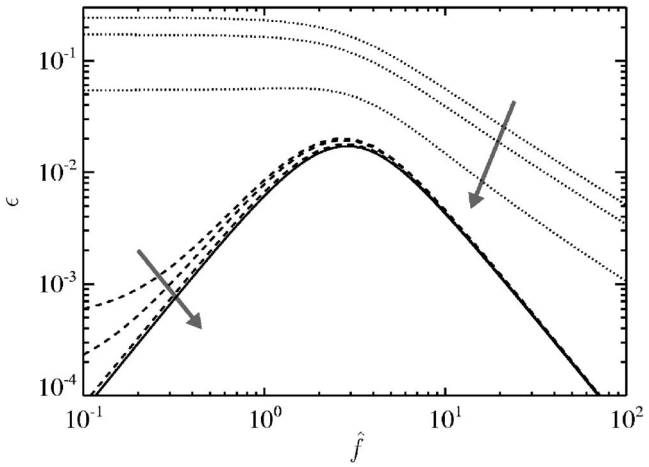

FIG. 12. Relative error in the average fractional extension between an approximate spring force law compared with an equal rod freely jointed chain, where the number of rods each spring represents is $\nu=4,6,20,\infty$ and the arrows denote increasing ν. The dotted lines are for the Cohen force law, the dashed lines are for the new approximate force law [Eq. (52)], and the solid line is the $\nu=\infty$ limit of both force laws. The force is nondimesionalized using the rod length, $\hat{f}=fA/k_BT$.

with the error of the Cohen form for comparison. The fourth moment of the spring length for the freely jointed chain is $\langle \hat{r}^4 \rangle_{eq}=(5\nu-2)/(3\nu^3)$. Again we see that the error of the approximate force law [Eq. (52)] is very small, only about 1% at $\nu=6$ and smaller at larger ν. The error has been reduced by about a factor of 40 below that of the Cohen force law.

The final property we analyze here is the force-extension behavior in the constant force ensemble. Recall that the response of the freely jointed chain in this ensemble is the Langevin function, $\langle \hat{z} \rangle = \mathcal{L}(\hat{f})$. We compare the error of the approximate force law and the Cohen force law in Fig. 12 for $\nu=4,6,20,\infty$. Note that the error does not exactly vanish in the limit $\nu \to \infty$ because the Cohen force law is not exactly the inverse Langevin function, although the error in fractional extension is less than 2% in that limit.

We have now developed and analyzed the error from using an approximate spring force law [Eq. (52)] to represent freely jointed chains. The error from using this approximate force law instead of the RWS model is small enough that the dominant error in a Brownian dynamics simulations will likely be from a nonzero integration time step and statistical error from a finite number of samples. *The error is small even when each spring represents only four rods.* It is important to emphasize that the new force law [Eq. (52)] outperforms the Cohen force law at all levels of discretization and so should be used instead of the Cohen force law by future simulators.

We can develop a similar approximate force law that models freely jointed chains with unequal rod lengths by proceeding in the exact same manner. As with the equal rod case, we will assume a form like the Cohen force law

$$\frac{f_s \bar{A}}{k_B T} = \frac{B\hat{r} + G\hat{r}^3}{1-\hat{r}^2}. \tag{53}$$

The values of B and G will depend on the number of rods and also the distribution of rod lengths. For the spring to have the correct limiting behavior at full extension we need

$$B + G = 2 - 4/\nu, \tag{54}$$

where here ν is defined using the average rod length, $\nu = \ell / \bar{A}$, which is equal to the total number of rods that the spring represents. For the equal rod case, we used the expansion of the second moment of the spring length for the approximate spring to get the remaining parameter B. Because the spring force takes the same form as the equal rod case, the expansion of the second moment of the spring length is the same

$$\langle \hat{r}^2 \rangle_{\text{eq}} \sim \frac{3}{\nu B} - \frac{30}{\nu^2 B^3} + \frac{30(24 - 7B + 2B^2)}{\nu^3 B^5} + \mathcal{O}\left(\frac{1}{\nu^4}\right). \tag{55}$$

We choose B in order to match this second moment with the second moment of the freely jointed chain. The second moment of the freely-jointed chain is $\langle \hat{r}^2 \rangle_{\text{eq}} = A_2 / \nu$, where A_2 is a function of the distribution of rod lengths and is defined as $A_2 \equiv \overline{A^2}/(\bar{A})^2$. Similarly we will define $A_4 \equiv \overline{A^4}/(\bar{A})^4$, which we will use later in discussing the fourth moment. By choosing

$$B = \frac{3}{A_2} - \frac{10A_2}{3\nu} + \frac{10A_2(4A_2^2 - 21A_2 + 18)}{27\nu^2}, \tag{56}$$

the second moment of the spring length for the approximate spring force law [Eq. (53)] is

$$\langle \hat{r}^2 \rangle_{\text{eq}} \sim \frac{A_2}{\nu} + \mathcal{O}\left(\frac{1}{\nu^4}\right). \tag{57}$$

The resulting approximate spring force law is

$$\frac{f_s \bar{A}}{k_B T} = \left[\frac{3}{A_2} - \frac{10A_2}{3\nu} + \frac{10A_2(4A_2^2 - 21A_2 + 18)}{27\nu^2}\right]\hat{r} + \frac{(2 - 4/\nu)\hat{r}^3}{1 - \hat{r}^2}. \tag{58}$$

In the limit $\nu \to \infty$ this becomes

$$\frac{f_s \bar{A}}{k_B T} = \frac{3}{A_2}\hat{r} + \frac{2\hat{r}^3}{1 - \hat{r}^2}. \tag{59}$$

We can quantify the accuracy of the approximate force-law by comparing the second and fourth moments of the spring length with the second and fourth moments for the underlying freely jointed chain. The fourth moment of the freely jointed chain is $\langle \hat{r}^4 \rangle_{\text{eq}} = (5A_2^2\nu - 2A_4)/(3\nu^3)$. Even when expressing a unequal rod system in terms of a few averages over the rods, the parameter space is large. We will quantify the error of the approximate spring force law for the same system shown in Fig. 5. This system consists of equal numbers of rods of length A and rods of length $5A$, resulting in $A_2 = 1.444$ and $A_4 = 3.862$. With these parameters fixed, we change the number of rods, and examine the error in the moments of the spring length in Fig. 13.

IV. SUMMARY AND OUTLOOK

We have examined a new method to generate coarse-grained models of polymers as bead-spring chains using the constant extension ensemble behavior of the polymer. We applied it to a number of toy problems to illustrate the mechanics of the method and important aspects of coarse-graining. Applying this method to the FJC polymer showed why current bead-spring chains are incapable of modeling polymers at high discretiza-

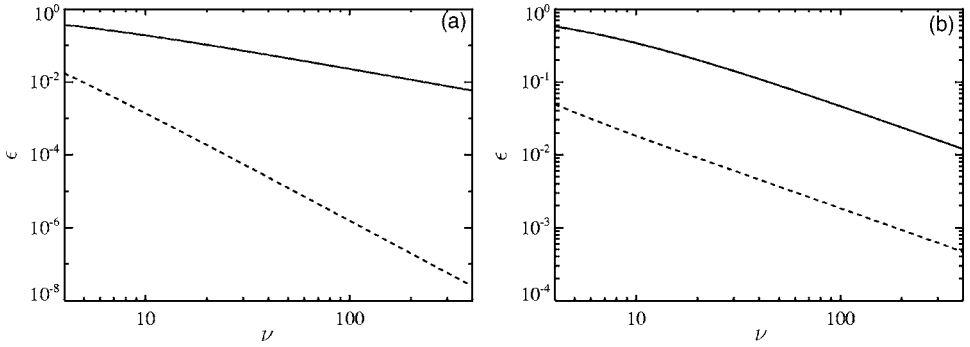

FIG. 13. Relative error in the equilibrium moments of the spring length between an approximate spring force law compared with an unequal rod freely jointed chain. The solid lines are for the Eq. (59) force law, and the dashed lines are for the new force law [Eq. (58)]. (a) Relative error in the second moment, $\langle \hat{r}^2 \rangle_{eq}$. (b) Relative error in the fourth moment, $\langle \hat{r}^4 \rangle_{eq}$.

tion. The analysis was applied to freely jointed chains in which the rods can have different lengths showing that as the spread in rod lengths increases, the response of the chain can change dramatically. This change cannot be accounted for solely by using an effective Kuhn length. We applied the method to construct a dumbbell model of actin filaments. This illustrated that the method in dumbbell form is applicable to the WLC as well as showing it can be used directly from experimentally data. These new force laws have a significant impact on not only the force-extension behavior but also the rheological behavior.

At the length and time scales that polymer kinetic theory aims to capture, the two common approaches are to use more detailed models such as the freely jointed chain or to use bead-spring chains where each bead represents a large segment of polymer. Because the current bead-spring models, such as the Cohen force law or Marko-Siggia force law, produce errors if they are pushed to high discretization, there exists a gap where there is no accurate coarse-grained version of the more detailed model. One method to reduce the size of this gap is to use an effective Kuhn length or persistence length. The use of this method has been examined in Underhill and Doyle (2004). This method has significant limitations including that there is not a unique, "correct" choice of the effective Kuhn or persistence length valid for all situations.

The advance of the PET method is that it bridges this gap in a systematic manner, showing how to calculate the force law at any level of coarse-graining. However, in practice the force laws calculated from the PET method may be difficult to implement. In these situations it may be sufficient to use an approximate force law. The approximate force law can have a simple functional form that is easy to use in calculations and captures the underlying model to high accuracy. We have shown examples of developing approximate force laws, including Eq. (52) which is capable of modeling a freely jointed chain to high discretization (springs representing as few as four Kuhn steps). Simulations that have used the Cohen force law can be easily modified to use this new force law, Eq. (52), including the semi-implicit predictor-corrector method developed by Somasi *et al.* (2002). Because the new force law is always better than the Cohen force law, Eq. (52) should always be used instead of the Cohen force law for modeling of freely jointed chains.

Similar to that development of an approximate force law as an alternative to the RWS

model, it appears useful to approximate the coupling behavior of worm-like chains using bending potentials. We hope that bead-spring chain models with bending potentials will be used in the future to fill the current gap for worm-like chains.

ACKNOWLEDGMENTS

This work was supported by the National Science Foundation CAREER Program Grant No. CTS-0239012 P.T.U. acknowledges support from the National Science Foundation Graduate Research Fellowship program.

References

Baschnagel, J., K. Binder, P. Doruker, A. Guusev, O. Hahn, K. Kremer, W. Mattice, F. Müller-Plathe, M. Murat, W. Paul, S. Santos, U. Suter, and V. Tries, "Bridging the gap between atomistic and coarse-grained models of polymers: Status and perspectives," Adv. Polym. Sci., **152**, 41–156 (2000).

Bird, R., C. Curtiss, R. Armstrong, and O. Hassager, *Dynamics of Polymeric Liquids, Volume 2: Kinetic Theory*, 2nd ed. (Wiley, New York, 1987).

Bustamante, C., J. Marko, E. Siggia, and S. Smith, "Entropic elasticity of λ-phage DNA," Science **265**, 1599–1600 (1994).

Cohen, A., "A Padé approximant to the inverse Langevin function," Rheol. Acta **30**, 270–272 (1991).

Dhar, A., and D. Chaudhuri, "Triple minima in free energy of semiflexible polymers," Phys. Rev. Lett. **89**, 065502 (2002).

Doyle, P., J. Bibette, A. Bancaud, and J.-L. Viovy, "Self-assembled magnetic matrices for DNA separation chips," Science **295**, 2237 (2002).

Doyle, P., B. Ladoux, and J.-L. Viovy, "Dynamics of a tethered polymer in shear flow," Phys. Rev. Lett. **84**, 4769–4772 (2000).

Flory, P., *Statistical Mechanics of Chain Molecules* (Oxford University Press, New York, 1989).

Foss, D., and J. Brady, "Brownian dynamics simulation of hard-sphere coloidal dispersions," J. Rheol. **44**, 629–651 (2000).

Han, J., and H. Craighead, "Separation of long DNA molecules in a microfabricated entropic trap array," Science **288**, 1026–1029 (2000).

Heyes, D., and J. Melrose, "Brownian dynamics simulations of model hard-sphere suspensions," J. Non-Newtonian Fluid Mech. **46**, 1–28 (1993).

Hur, J., E. Shaqfeh, and R. Larson, "Brownian dynamics simulations of single DNA molecules in shear flow," J. Rheol. **44**, 713–742 (2000).

Jendrejack, R., E. Dimalanta, D. Schwartz, M. Graham, and J. de Pablo, "DNA dynamics in a microchannel," Phys. Rev. Lett. **91**, 038102 (2003).

Keller, D., D. Swigon, and C. Bustamante, "Relating single-molecule measurements to thermodynamics," Biophys. J. **84**, 733–738 (2003).

Kratky, O., and G. Porod, "X-ray investigation of dissolved chain molecules," Recl. Trav. Chim. Pays-Bas **68**, 1106–1022 (1949).

Larson, R., T. Perkins, D. Smith, and S. Chu, "Hydrodynamics of a DNA molecule in a flow field," Phys. Rev. E **55**, 1794–1797 (1997).

Le Goff, L., O. Hallatschek, E. Frey, and F. Amblard, "Tracer studies of F-actin fluctuations," Phys. Rev. Lett. **89**, 258101 (2002).

Marko, J., and E. Siggia, "Stretching DNA," Macromolecules **28**, 8759–8770 (1995).

Öttinger, H., *Stochastic Processes in Polymeric Fluids: Tools and Examples for Developing Simulation Algorithms* (Springer, Berlin, 1996).

Pathria, R., *Statistical Mechanics*, 2nd ed. (Butterworth-Heinemann, Boston, 1996).

Rayleigh, Lord, "On the problem of random vibrations, and of random flights in one, two or three dimensions,"

Philos. Mag. **37**, 321–347 (1919).

Samuel, J., and S. Sinha, "Elasticity of semiflexible polymers," Phys. Rev. E **66**, 050801 (2002).

Somasi, M., B. Khomami, N. Woo, J. Hur, and E. Shaqfeh, "Brownian dynamics simulations of bead-rod and bead-spring chains: Numerical algorithms and coarse-graining issues," J. Non-Newtonian Fluid Mech. **108**, 227–255 (2002).

Treloar, L., *The Physics of Rubber Elasticity, 2nd ed.* (Clarendon, Oxford, 1975).

Underhill, P., and P. Doyle, "On the coarse-graining of polymers into bead-spring chains," J. Non-Newtonian Fluid Mech. **122**, 3–31 (2004).

Warner, H., "Kinetic theory and rheology of dilute suspensions of finitely extendible dumbbells," Ind. Eng. Chem. Fundam. **11**, 379–387 (1972).

Wilhelm, J., and E. Frey, "Radial distribution function of semiflexible polymers," Phys. Rev. Lett. **77**, 2581–2584 (1996).